Scientific Research Publishing

Numerical Study of Methane Dry Reforming Reaction in a Disk Reactor with Focused Solar Simulator

Yarong Wang[1], Jing Ding[2], Jianfeng Lu[2]*

[1]School of Intelligent Systems Engineering, Sun Yat-sen University, Guangzhou, China
[2]School of Materials and Engineering, Sun Yat-sen University, Guangzhou, China
Email: *lujfeng@mail.sysu.edu.cn

Abstract

Heat transfer and thermochemical energy storage process of methane dry reforming in a disk reactor with focused solar simulator was modeled and analyzed. The results showed that thermochemical energy storage efficiency of disk reactor can reach 28.4%, and that is higher than that of tubular reactor. The maximum reaction rate occurs at catalyst bed corner near the baffle, because the corner has high temperature and high reactant molar fraction. As reactant flow increases, methane conversion and thermochemical energy storage efficiency decrease as catalyst bed temperature and heat loss decrease. The thermochemical energy storage efficiency increased first and then decreased with methane molar ratio increasing, while methane conversion and the thermochemical energy storage efficiency increased with reactant temperature increasing. As catalyst bed porosity rises, methane conversion and thermochemical energy storage efficiency increased first and then decreased, and optimum porosity is 0.31.

Keywords

Methane Dry Reforming, Thermochemical Energy Storage, Focused Solar Simulator, Disk Reactor

1. Introduction

Solar energy is a kind of abundant clean energy, but the cost of energy development and utilization is high and the efficiency is low due to its dispersion and instability. Thermochemical energy storage technology is the most promising high-temperature energy storage method. Research in the past two decades has

shown that solar thermal energy can effectively drive chemical conversion reactions [1] [2]. Methane dry reforming thermochemical energy storage is a form of efficient energy utilization that can convert solar energy into stable chemical combustion energy [1]. Its main advantages [2] include large storage capacity per unit of methane, high temperature reaction condition (>600˚C), and full use of greenhouse gases CH_4 and CO_2.

In recent years, solar reforming reactors are mainly developed into three types: indirectly heated reformer, tubular reformer-receiver and the windowed or volumetric reformer-receiver [3]. ASTERIX [4] [5] carried out solar steam reforming experiment of methane in the early 1990s, and studied details and related problems of process heat demand of industrial chemical process with solar energy and high temperature using indirect heating converter. The catalytically enhanced solar absorption receiver (CAESAR) [6] [7] test was used to determine the thermal, chemical, and mechanical properties of a commercial scale dish-shaped direct catalytic absorption receiver reactor under a series of steady-state and transient operating conditions. In order to perform an efficient carbon dioxide and water vapor reforming reaction, Weizmann Institute of Science designed a solar receiver with storage and transportation for high-temperature technology development, and tested it in a 480 kW reformer [8]. Jin *et al.* [9] proposed a methane reforming reactor with a compound paraboloid concentrator and a mesh porous ceramic. The simulation results show that compared with the traditional reactor design, the reactor design proposed in this study can improve the photochemical efficiency of solar methane conversion.

In addition to experimental research, the researchers conducted a large number of numerical simulation studies. Rubin *et al.* [10] proposed a numerical model based on Arrhenius equation for simulating methane steam reforming, and simulation results were in agreement with experimental results. Akpan *et al.* [11] established a reaction kinetics model for carbon dioxide methane reforming under Ni/CeO_2-ZrO_2 catalyst through experiments and simulations. Akbanri *et al.* [12] established a three-dimensional microreactor model for simulating methane autothermal reforming in fuel cells, and studied the effects of airspeed, air/fuel ratio, water-fuel ratio and inlet temperature on the reaction. Wang *et al.* [13] [14] [15] used combined method with Monte Carlo Ray Tracing method and Finite Volume Method to establish heat and mass transfer model coupled with thermochemical reaction kinetics for porous medium solar thermochemical reactor. The numerical results showed that concentrated solar irradiation affects reactor thermal performance, methane steam reforming chemical reaction rate and hydrogen production. Gu *et al.* [16] analyzed heat transfer and storage performance of steam methane reforming in tubular reactor with focused solar simulator by measurement and simulation. Fernando *et al.* [17] found that methane steam reforming in a fixed-bed reactor can efficiently store thermal energy in high temperature. Benguerba *et al.* [18] analyzed the effect of using different

temperatures on the methane dry reforming performance in a fixed-bed catalytic reactor by a one-dimensional heterogeneous model.

At present, the research on methane dry reforming thermochemical energy storage process in enhanced reactor still need to be further investigated. In this paper, the thermochemical storage performance of methane dry reforming disk reactor was studied with focused solar simulator. The reactant flow, reactant methane molar ratio, reactant temperature and catalyst bed porosity were analyzed for mechanism of methane dry reforming process in the disk reactor, to find a new method to improve the methane conversion and energy storage efficiency of the system.

2. Numerical Model

2.1. Model Introduction

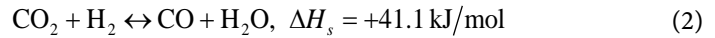**Figure 1** describes physical model of a methane dry reforming disk reactor with
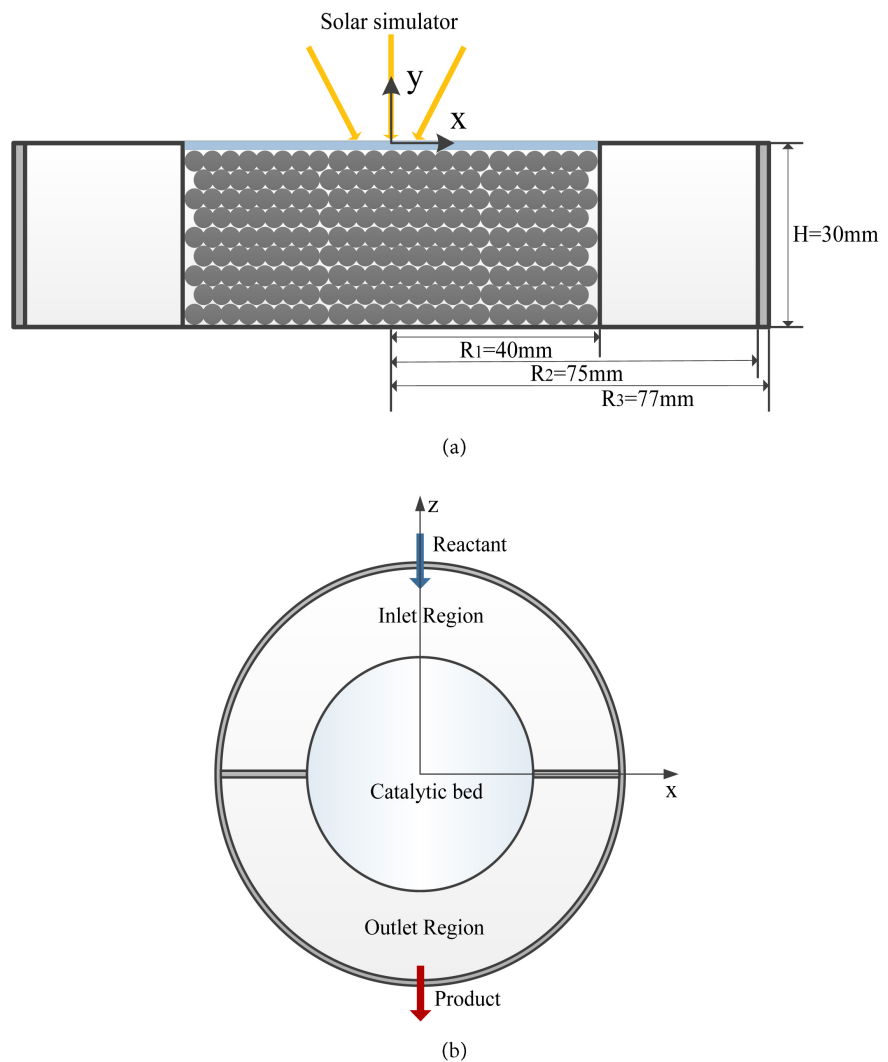
Figure 1. Physical model of disk reactor with solar simulator. (a) x = 0 section, (b) y = 0 section.

focused solar simulator. The reformer is a disk with radius of R_3 and height of H, and catalyst is also a disk with radius of R_1. The inlet region and outlet region are separated by catalyst bed and two baffles. The outer surface with quartz glass at $y = 0$ is heated by concentrated heat flow from solar simulator.

The main reaction of methane dry reforming reaction is:

$$CH_4 + CO_2 \leftrightarrow 2CO + 2H_2, \quad \Delta H_m = +247.3 \, \text{kJ/mol} \tag{1}$$
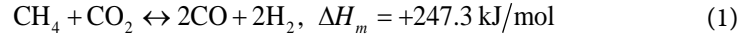
The main side reaction is:

$$CO_2 + H_2 \leftrightarrow CO + H_2O, \quad \Delta H_s = +41.1 \, \text{kJ/mol} \tag{2}$$

Inlet mole fraction of methane is:

$$y = \frac{F_{CH_4,i}}{F_{CH_4,i} + F_{CO_2,i}} \tag{3}$$

where $F_{CH_4,i}$ and $F_{CO_2,i}$ denote inlet flow rates of methane and carbon dioxide under standard condition (1 atm, 20˚C), respectively.

Methane conversion is:

$$X_{CH_4} = \frac{F_{CH_4,i} - F_{CH_4,o}}{F_{CH_4,i}} \tag{4}$$

where $F_{CH_4,o}$ is methane outlet flow under standard condition.

Carbon dioxide conversion rate is:

$$X_{CO_2} = \frac{F_{CO_2,i} - F_{CO_2,o}}{F_{CO_2,i}} \tag{5}$$

where $F_{CO_2,o}$ is carbon dioxide outlet flow under standard condition.

The energy flow received by reactor from solar simulator is:

$$E_{in} = \iint_{S_w} q_r \, \text{d}S \tag{6}$$

where q_r is concentrated radiant heat flux on reactor surface, S_w is surface area of reactor irradiate by solar simulator.

$$q_r = q_c \exp\left(-1464.3 r^2\right) \tag{7}$$

where q_c denotes central heat flux, and r denotes radius from focus.

Thermochemical energy storage is:

$$Q_{ch} = \frac{F_{CH_4} \cdot X_{CH_4} \cdot \Delta H_m}{v_{CH_4}} + \frac{F_{CO_2} \cdot \left(X_{CO_2} - X_{CH_4}\right) \cdot \Delta H_s}{v_{CO_2}} \tag{8}$$

where v denote mole volume under standard condition. ΔH_m and ΔH_s are reaction heat of main reaction and side reaction.

Sensible heat increment is [18]:

$$Q_{se} = \sum_i \int_{T_s}^{T_0} F_{o,i} \rho_{o,i} c_{p,o,i} \, \text{d}T \tag{9}$$

where $\rho_{o,i}$, $c_{p,o,i}$ are density and specific heat of species i in product, T_s and T_0 are surrounding and outlet temperatures.

Thermochemical energy storage efficiency and total energy storage efficiency are:

$$\eta_{ch} = \frac{Q_{ch}}{E_{in}} \quad (10)$$

$$\eta_{total} = \frac{Q_{total}}{E_{in}} = \frac{Q_{ch} + Q_{se}}{E_{in}} \quad (11)$$

2.2. Theoretical Assumption and Model

Based on existing experimental data, a three-dimensional model of disk reactor with solar simulator is established. The entire process is assumed to be steady, and fluid is assumed to be ideal gas. The model contains solid domain of reactor wall, fluid domain with porous media inside reactor. Catalyst bed is assumed as porous media.

The fluid zone includes inlet and outlet regions, and porous zone of catalyst bed. Continuity equation can be expressed as:

$$\frac{\partial \left(\rho_f u_i \right)}{\partial x_i} = 0 \quad (12)$$

where ρ_f is density of mixed fluid, u_i is superficial velocity vector based on the total cross-sectional area of fluid and porous medium.

Momentum conservation equation is expressed as:

$$\frac{\partial}{\partial x_j} \left(\rho_f u_i u_j \right) = \frac{\partial}{\partial x_j} \left(\mu \frac{\partial u_i}{\partial x_j} \right) - \frac{\partial p}{\partial x_i} + \rho_f g_i + S_{m,i} \quad (13)$$

where μ is dynamic viscosity, p is fluid pressure, g_i is gravitational acceleration and $S_{m,i}$ is momentum source caused by flow in porous media. In the inlet and outlet regions, $S_{m,i} = 0$.

The momentum source for homogeneous porous media consists of viscosity loss term and inertia term as [19]:

$$S_{m,i} = \left(\frac{\mu}{\alpha} u_i + C_2 \frac{1}{2} \rho_f |u| u_i \right) \quad (14)$$

The permeability and internal resistance factor [20] can be calculated as:

$$\alpha = \frac{D_p^2}{150} \frac{\gamma^3}{\left(1 - \gamma \right)^2} \quad (15)$$

$$C_2 = \frac{3.5}{D_p} \frac{1 - \gamma}{\gamma^3} \quad (16)$$

where D_p is the diameter of catalyst particles.

During chemical reaction process, the fractions of reactants and products change, and mass transport equation is [19]:

$$\frac{\partial}{\partial x_j} \left(\rho_f Y_i u_j \right) + \frac{\partial J_{i,j}}{\partial x_j} = r_i \quad (17)$$

where Y_i, $J_{i,j}$ and r_i are respectively mass fraction, diffusion flux and reaction rate for species.

Chemical reaction is assumed as volumetric reaction, and the reaction rate is calculated by standard Arrhenius equation as:

$$k = A\mathrm{e}^{-E_a/RT} \tag{18}$$

where A and E_a mean pre-reaction factor and activation energy.

In solid zone of reactor wall, heat transfer is controlled by heat conduction, and its governing equation is:

$$\frac{\partial}{\partial x_i}\left(k_w \frac{\partial T_w}{\partial x_i}\right) = 0 \tag{19}$$

where T_w is temperature of reactor wall, and k_w is the thermal conductivity.

In fluid zone, energy conservation equation can be expressed as:

$$\frac{\partial}{\partial x_i}\left(\rho_f c_p u_i T\right) = \frac{\partial}{\partial x_i}\left(k_{eff} \frac{\partial T}{\partial x_i}\right) + S_h \tag{20}$$

where S_h is energy source caused by chemical reaction, and k_{eff} is effective conductivity. S_h is directly calculated by enthalpy difference of reactants and products.

The effective thermal conductivity is calculated as volume average of thermal conductivities of fluid and solid as [21]:

$$k_{eff} = \gamma k_f + (1-\gamma)k_s \tag{21}$$

where k_f and k_s are conductivity of fluid and porous medium, respectively.

The heat loss from the reactor wall is primarily determined by natural convection and radiation. The boundary condition for heating surface is:

$$-k_w \nabla T_w = h_n (T_w - T_s) + \varepsilon\sigma\left(T_w^4 - T_s^4\right) - q_r \tag{22}$$

where h_n is heat transfer coefficient of natural convection, σ is black body radiation constant, ε is emissivity, and T_s is surrounding temperature.

The boundary condition of back surface is:

$$-k_w \nabla T_w = h_n (T_w - T_s) + \varepsilon\sigma\left(T_w^4 - T_s^4\right) \tag{23}$$

2.3. Calculation Condition and Model Validation

According to the experimental results, the pre-exponential factor and activation energy of the main reaction are $A_1 = 1.2 \times 10^7$ and $Ea_1 = 5.8 \times 10^7 \, \mathrm{J/kmol}$, and those of side reaction are $A_2 = 31900$ and $Ea_2 = 1.69 \times 10^7 \, \mathrm{J/kmol}$. The heating surface of the reactor is affected by the air-cooling system, and $h_h = 12.6 \, \mathrm{W/m^2 \cdot K}$, while convective heat transfer coefficient on back side is $h_h = 4 \, \mathrm{W/m^2 \cdot K}$. The emissivity ε of the outer wall surface of the reactor is 0.93, the ambient temperature was 25°C, and the flow of the reactant inlet was uniform.

Yu *et al.* [22] experimentally measured tubular methane dry reforming reactor

based on solar radiation, which is similar to present model. Table 1 shows comparison of experimental and simulation results of methane conversion and thermochemical storage efficiency at different conditions. The results show that present numerical model is effective, and methane dry reforming energy storage system can be further analyzed.
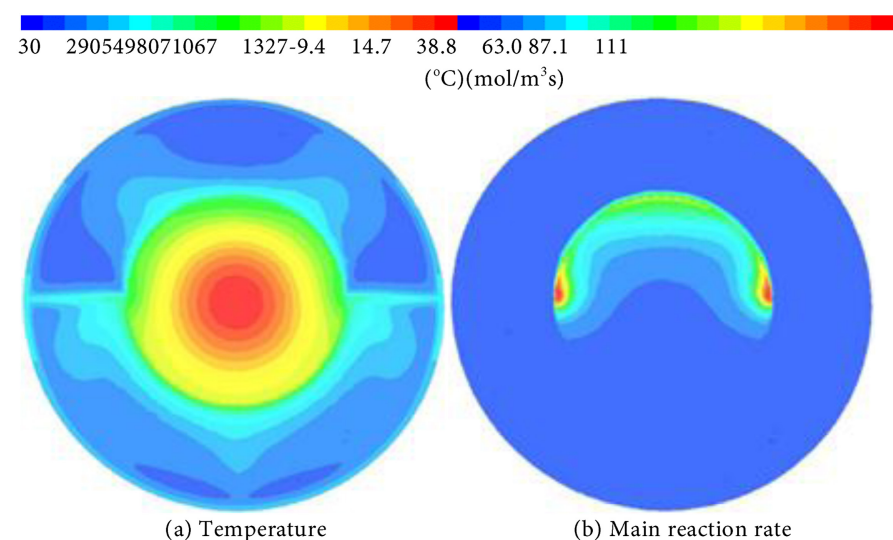
3. Results and Discussions

3.1. Heat and Mass Transfer

Figure 2 shows temperature and main reaction rate distribution of disk reactor. The heat flux distribution of solar simulator conforms to Gaussian distribution, resulting in high energy near the focus which causes high temperature, so the temperature of catalyst bed is a corresponding circular distribution from the center to boundary. Figure 3 shows molar fraction distribution of

Table 1. Simulation and experimental comparison [22].

Condition ($\gamma = 0.5$)	Methane conversion (%)			Thermochemical energy storage efficiency (%)		
	Experiment	Simulation	Relative error	Experiment	Simulation	Relative error
$q_c = 702$ kW/m², $F = 3$ L/min	30.9	30.0	-2.90	4.02	3.69	8.15
$q_c = 714$ kW/m², $F = 4$ L/min	36.2	38.3	5.81	5.74	6.10	-6.34
$q_c = 678$ kW/m², $F = 6$ L/min	40.5	43.5	7.29	10.1	10.9	-7.66

30   290 549 807 1067   1327 -9.4   14.7   38.8   63.0 87.1   111
(°C)(mol/m³s)

(a) Temperature   (b) Main reaction rate

Figure 2. Cloud map of temperature and main reaction in heated surface ($q_c = 478$ kW/m², $\gamma = 0.5$, $F = 3$ L/min).

(a) CH$_4$ (b) H$_2$
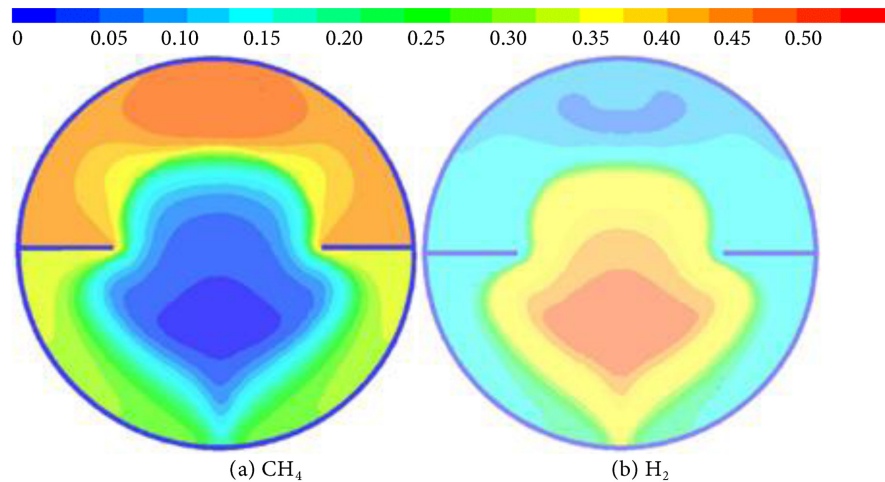
Figure 3. Cloud map of molar fraction (q_c = 478 kW/m², y = 0.5, F = 3 L/min).

mixed gas. The main reaction rate reaches the maximum value at the corner of the catalyst bed near the baffle and decreases toward the center, because reactant molar fraction as methane increase correspondingly from the center to the boundary, while product molar fraction as hydrogen decrease from the center to the boundary.

Figure 4 shows parameter change in radial direction of catalyst bed. In top boundary of catalyst bed, the temperature corresponds to the distribution of incident energy flux, which gradually decreases from center to boundary. The main reaction rate first increases and then decreases in radial direction, and reaches a maximum value at the corner of catalyst bed baffle of x = 38.7 mm for the accumulation of reactants near the corners of catalyst bed baffle.

3.2. Effect of Reactant Flow

Figure 5 describes the changes of methane conversion and thermochemical storage efficiency with reactant flow in disk reactor system. As the reactant flow increases, catalyst bed temperature and mixed gas outlet temperature decrease, and conversion of methane and carbon dioxide both are reduced, while the thermochemical energy storage efficiency increases. Figure 6 describes the energy ratio of disk reactor as a function of reactant flow. As reactant flow increases, although the mixture gas outlet temperature decreases slightly, the sensible heat storage efficiency increases due to the increase in the total gas volume. The heat loss is reduced for wall temperature decreasing, so the total energy storage efficiency increases.
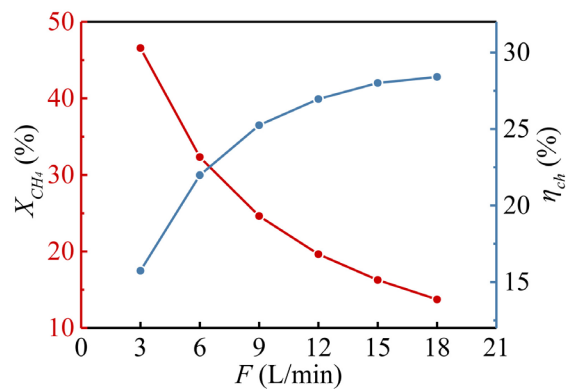
3.3. Effect of Reactant Mole Fraction

Figure 7 presents methane conversion and storage efficiency in disk reactor with different methane molar ratio. As methane molar ratio of reactants increases, methane conversion gradually decreases. The thermochemical energy storage efficiency and total energy storage efficiency increase first and then decrease as

(a)

(b)
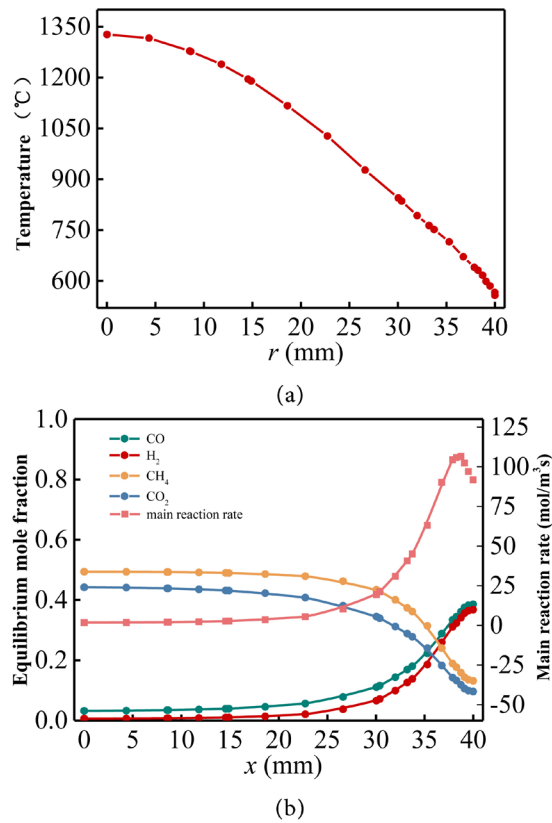
Figure 4. Parameter change in radial direction of catalyst bed (q_c = 478 kW/m^2, y = 0.5, F = 3 L/min). (a) Temperature, (b) Molar fraction and main reaction rate.


Figure 5. Methane conversion and thermochemical energy storage efficiency in disk reactor with different reactant flow (q_c = 478 kW/m^2, y = 0.5).

methane molar ratio increases, reaching a maximum value at y = 0.5, which is due to the best chemical reaction rate under the ideal molar ratio.
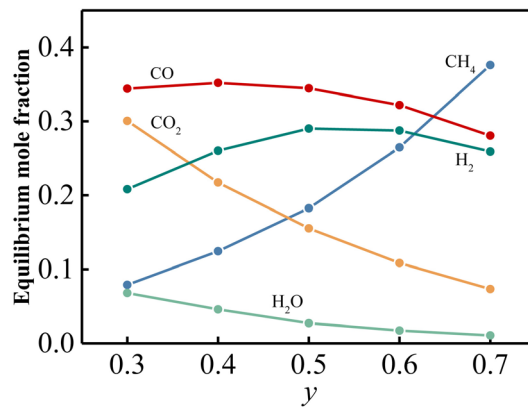
Figure 8 presents molar fraction in disk reactor. Increasing the proportion of carbon dioxide can promote the reverse reaction of water vapor shift reaction. As methane molar ratio of reactants increases, the amount of carbon dioxide gradually decreases, which reduces the likelihood of the reverse reaction of the
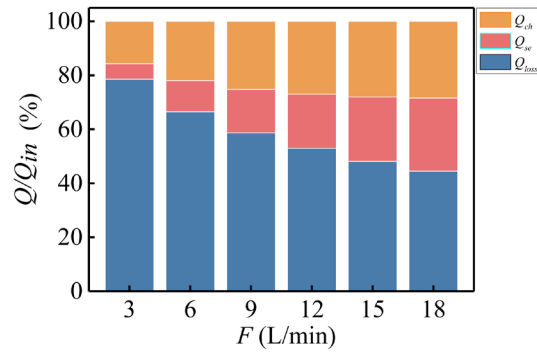
Figure 6. Energy ratio of disk reactor with different reactant flow (q_c = 478 kW/m², y = 0.5).
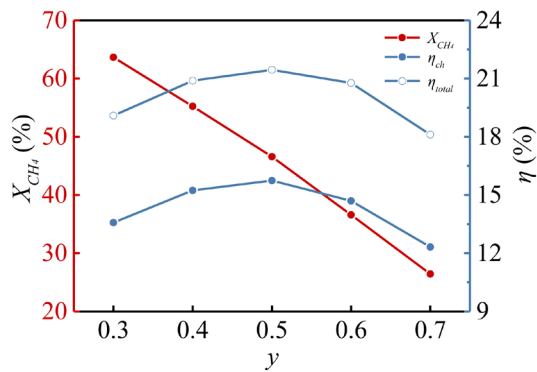
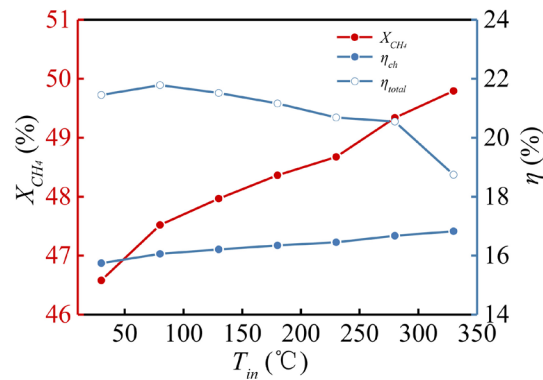**Figure 7.** Methane conversion and storage efficiency with different methane molar ratio in disk reactor (q_c = 478 kW/m², F = 3 L/min).

Figure 8. Molar fraction in disk reactor with different methane molar ratio (q_c = 478 kW/m², F = 3 L/min).

water vapor shift reaction going forward, thus the amount of by-product H_2O produced will decrease. On the other hand, the production of H_2 gets the maximum at y = 0.5 under the ideal molar ratio.

3.4. Effect of Reactant Temperature

Figure 9 describes methane conversion and energy storage efficiency in disk

Figure 9. Simulation diagram of methane conversion and energy storage efficiency with reactant temperature in a disk reactor system (q_c = 478 kW/m^2, y = 0.5, F = 3 L/min).

reactor with different reactant temperature. As reactant temperature rises, methane conversion increases, because inside catalyst bed temperature increases, and then the reaction rate and methane conversion increase accordingly. Since the catalyst bed temperature in reactor does not increase significantly with the increase of reactant temperature, the sensible energy storage decreases significantly. Therefore, the thermochemical energy storage efficiency increases, and the total energy storage efficiency increases slightly and then gradually decreases, as shown in Figure 10.

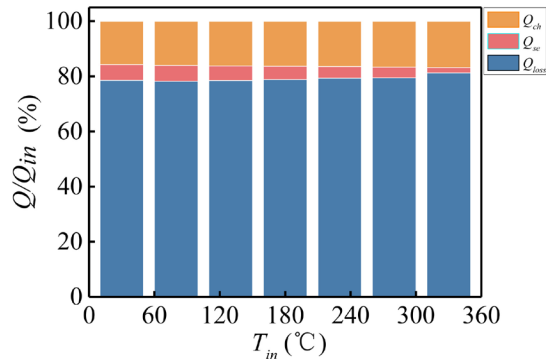## 3.5. Effect of Catalyst Bed Porosity

The porosity of catalyst bed has important effect on heat and mass transfer process inside the reactor. Figure 11 describes methane conversion and thermochemical energy storage efficiency in disk reactor with different catalyst bed porosity. The methane conversion and thermochemical energy storage efficiency both increase first and then decrease with the increase of catalyst bed porosity, and the optimal porosity is 0.31.

4. Conclusions

In this paper, heat transfer and energy storage performance of methane carbon dioxide disk reactor with concentrated heat flux were numerically studied, and conclusions are as follows:

1) The thermochemical energy storage efficiency of disk reactor can reach 28.4%, and that is remarkably higher than that of traditional tube reactor.

2) The maximum reaction rate occurs at catalyst bed corner near the baffle, because catalyst bed corner has high temperature and high reactant molar fraction.

3) The trends of methane conversion and thermochemical energy storage efficiency are similar. As the reactant flow increases, methane conversion and thermochemical energy storage efficiency decrease as catalyst bed temperature

Figure 10. Simulation diagram of energy ratio of disk reactor with reactant temperature ($q_c = 478$ kW/m², $y = 0.5$, $F = 3$ L/min).
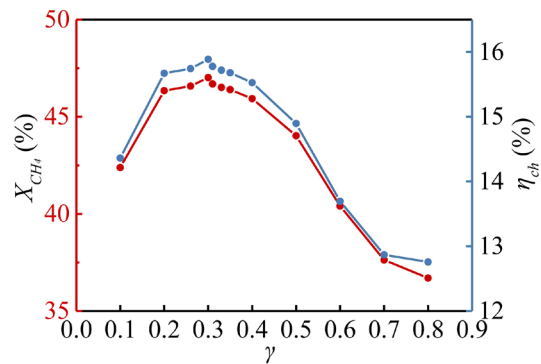
Figure 11. Methane conversion and thermochemical energy storage efficiency in disk reactor with catalyst bed porosity ($q_c = 478$ kW/m², $y = 0.5$, $F = 3$ L/min).

and heat loss decrease.

4) Increasing reactant temperature is conducive to improving methane conversion and thermochemical energy storage efficiency.

5) As catalyst bed porosity increases, methane conversion and thermochemical storage efficiency increase first and then decrease, and optimum porosity is 0.31.

Acknowledgements

Conflicts of Interest

The authors declare no conflicts of interest regarding the publication of this paper.

References

[1] Dai, L., Long, X.F., Lou, B., Zhou, S.Q. and Xu, Y. (2018) Progress in Thermochem-

ical Energy Storage for Concentrated Solar Power: A Review. *International Journal of Energy Research*, **42**, 4546-4561. https://doi.org/10.1002/er.4183

[2]   Wang, X.H., Du, X.C. and Wei, J.J. (2017) Research Progress of Different Solar Thermochemical Energy Storage Systems. *Chinese Science Bulletin*, **62**, 3631-3642. https://doi.org/10.1360/N972017-00398

[3]   Spiewak, I., Tyner, C.E. and Langnickel, U. (1993) Applications of Solar Reforming Technology. https://doi.org/10.2172/10131314

[4]   Manfred, B., Ulrich, L. and Manuel, S. (1991) Solar Steam Reforming of Methane. *Solar Energy Materials*, **43**, 441-448. https://doi.org/10.1016/0165-1633(91)90081-U

[5]   Böhmer, M., Langnickel, U. and Sanchez, M. (1991) Solar Steam Reforming of Methane. *Solar Energy Materials*, **24**, 441-448. https://doi.org/10.1016/0165-1633(91)90081-U

[6]   Buck, R., Muir, J.F. and Hogan, R.E. (1991) Carbon Dioxide Reforming of Methane in a Solar Volumetric Receiver/Reactor: The CAESAR Project. *Solar Energy Materials*, **24**, 449-463. https://doi.org/10.1016/0165-1633(91)90082-V

[7]   Muir, J.F., Hogan Jr., R.E., Skocypec, R.D. and Buck, R. (1991) Solar Reforming of Methane in a Direct Absorption Catalytic Reactor on a Parabolic Dish: I—Test and Analysis. *Solar Energy*, **52**, 467-477. https://doi.org/10.1016/0038-092X(94)90654-8

[8]   Spiewak, I., Epstein, M. and Segal, A. (1991) The Weizmann Institute of Science 480-kW Reformer System. IEA SSPS Task V. *Proceedings of the Workshop on Methane Reforming*, Koeln, 11-13 June 1991, 129-137.

[9]   Jin, J., Wei, X., Liu, M.K., Yu, Y.H., Li, W.J., Kong, H. and Hao, Y. (2018) A Solar Methane Reforming Reactor Design with Enhanced Efficiency. *Applied Energy*, **226**, 797-807. https://doi.org/10.1016/j.apenergy.2018.04.098

[10] Rubin, R., Karni, J. and Yeheskel, J. (2004) Chemical Kinetics Simulation of High Temperature Hydrocarbons Reforming in a Solar Reactor. *Journal of Solar Energy Engineering*, **126**, 858-866. https://doi.org/10.1115/1.1691439

[11] Akpan, E., Sun, Y., Kumar, P., *et al*. (2007) Kinetics, Experimental and Reactor Modeling Studies of the Carbon Dioxide Reforming of Methane (CDRM) over a New Ni/CeO_2-ZrO_2 Catalyst in a Packed Bed Tubular Reactor. *Chemical Engineering Science*, **62**, 4012-4024. https://doi.org/10.1016/j.ces.2007.04.044

[12] Akbari, M.H., Ardakani, A.H. and Tadbir, M.A. (2011) A Microreactor Modeling, Analysis and Optimization for Methane Autothermal Reforming in Fuel Cell Applications. *Chemical Engineering Journal*, **166**, 1116-1125. https://doi.org/10.1016/j.cej.2010.12.044

[13] Wang, F.Q., Shuai, Y., Wang, Z.Q., Leng, Y. and Tan, H.P. (2014) Thermal and Chemical Reaction Performance Analyses of Steam Methane Reforming in Porous Media Solar Thermochemical Reactor. *International Journal of Hydrogen Energy*, **39**, 718-730. https://doi.org/10.1016/j.ijhydene.2013.10.132

[14] Wang, F.Q., Tan, J.Y., Shuai, Y., Gong, L. and Tan, H.P. (2014) Numerical Analysis of Hydrogen Production via Methane Steam Reforming in Porous Media Solar Thermochemical Reactor Using Concentrated Solar Irradiation as Heat Source. *Energy Conversion and Management*, **87**, 956-964. https://doi.org/10.1016/j.enconman.2014.08.003

[15] Wang, F.Q., Tan, J.Y., Ma, L.X. and Leng, Y. (2015) Effects of Key Factors on Solar Aided Methane Steam Reforming in Porous Medium Thermochemical Reactor. *Energy Conversion and Management*, **103**, 419-430. https://doi.org/10.1016/j.enconman.2015.06.049

[16] Gu, R., Ding, J., Wang, Y.R., *et al.* (2019) Heat Transfer and Storage Performance of Steam Methane Reforming in Tubular Reactor with Focused Solar Simulator. *Applied Energy*, **233**, 789-801. https://doi.org/10.1016/j.apenergy.2018.10.072

[17] Fernando, A.A.S., Kenia, C.M. and Jornandes, D.S. (2016) A Simulation Study of the Steam Reforming of Methane in a Fixed-Bed Reactor. *Engineering*, **8**, 245-256. https://doi.org/10.4236/eng.2016.84021

[18] Benguerba, Y., Dehimi, L., Virinie, M., Dumas, C. and Ernst, B. (2015) Modelling of Methane Dry Reforming over Ni/Al_2O_3 Catalyst in a Fixed-Bed Catalytic Reactor. *Reaction Kinetics Mechanisms and Catalysis*, **114**, 109-119. https://link.springer.com/article/10.1007/s11144-014-0772-5

[19] Fluent 6.3 Documentation. http://www.fluent.com

[20] Ergun, S. (1952) Fluid Flow through Packed Columns. *Chemical Engineering Progress*, **48**, 89-94.

[21] Alazmi, B. and Vafai, K. (2000) Analysis of Variants within the Porous Media Transport Models. *Journal of Heat Transfer*, **122**, 303-326. https://doi.org/10.1115/1.521468

[22] Yu, T., Yuan, Q.Q., Lu, J.F., Ding, J. and Lu, Y.L. (2017) Thermochemical Storage Performances of Methane Reforming with Carbon Dioxide in Tubular and Semi-Cavity Reactors Heated by a Solar Dish System. *Applied Energy*, **185**, 1994-2004. https://doi.org/10.1016/j.apenergy.2015.10.131